Journal of Materials Chemistry C

PAPER

View Article Online
View Journal | View Issue

Cite this: J. Mater. Chem. C, 2016, 4, 2606

Efficient polymer solar cells based on a new quinoxaline derivative with fluorinated phenyl side chain†

Qunping Fan,[a] Huanxiang Jiang,[b] Yu Liu,*[ac] Wenyan Su,[a] Hua Tan,[a] Yafei Wang,[a] Renqiang Yang*[b] and Weiguo Zhu*[ac]

Received 25th January 2016,
Accepted 2nd March 2016

DOI: 10.1039/c6tc00353b

www.rsc.org/MaterialsC

A novel donor–π–acceptor (D–π–A) type polymer of **PBDTT-DTFPQx** composed of a medium electron-donating 5,8-dialkylthienyl substituted benzo[1,2-*b*:4,5-*b*′]dithiophene (BDTT) moiety and a strong electron-accepting 4-fluorophenyl substituted 6,7-dioctyloxyquinoxaline (FPQx) with thiophene π-bridge units was synthesized and characterized, as a donor material for polymer solar cells (PSCs). This polymer exhibits a low optical bandgap of 1.66 eV with an absorption onset of 745 nm, a low-lying HOMO energy level of −5.52 eV, and a hole mobility of 5.05×10^{-4} cm^2 V^{-1} s^{-1}. Compared to the reported analogues, PSCs based on **PBDTT-DTFPQx**/$PC_{71}BM$ demonstrated an outstanding fill factor (FF) value. With an optimized blend ratio of PBDT-TFQ : $PC_{71}BM$ (1 : 4, w/w), a high power conversion efficiency (PCE) of 7.2% was obtained, with an open-circuit voltage (V_{oc}) of 0.87 V, a short-circuit current (J_{sc}) of 11.4 mA cm^{-2}, and a FF of up to 73% under AM 1.5G irradiation. The results demonstrate that the introduction of two fluoride atoms onto 4-positions of the phenyl group at the quinoxaline unit by side-chain engineering into the BDTT-*alt*-DTQx type polymers would be a feasible approach to improve photovoltaic properties in PSCs.

1. Introduction

As a promising sustainable energy source technology for future, bulk heterojunction (BHJ) polymer solar cells (PSCs), which are based on the blending of polymers/fullerene derivatives materials in the bulk active layer of the devices, have recently attracted tremendous interest due to their advantages of low cost, light weight, flexibility, ease of processing and large area mass production.[1–4] To improve the photovoltaic performance of PSCs, tremendous efforts have been devoted to develop new solution processable donor–acceptor (D–A) type polymer donor materials with narrow optical bandgap, with low highest occupied molecular orbital (HOMO) levels and high carrier mobility.[5–9] Encouragingly, a record power conversion efficiency (PCE) of up to 10.8% had been achieved by PSCs with a delicate balance among the three factors of optical bandgap, energy level and carrier mobility *via* sophisticated control over the physical and electro-chemistry properties.[10] Despite some remarkable advancements of the conjugated polymers having been achieved, there remain some challenges to overcome for highly efficient PSCs, especially with respect to most D–A alternating polymers being unable to obtain a high PCE due to the imbalance among open-circuit voltage (V_{oc}), short-circuit current density (J_{sc}) and fill factor (FF).[11–13] As is known to all, sometimes a lower HOMO level of the donor materials can lead to an increased optical bandgap (E_g^{opt}) and a decreased J_{sc}.[13–15] That is, a high V_{oc}, J_{sc} and FF are difficult to obtain concurrently, especially the FF is low in most cases.[16]

As is well-known, a conjugated polymer is mostly made up of two parts: the π-conjugated backbones and the side chains, where the π-conjugated backbones mainly determine the opto-electronic properties of the resulting polymers. Until now, lots of different backbones have been reported.[1,2] Meanwhile, side chain engineering is indeed an essential and widespread technique used to tune the physical properties of a conjugated polymer to achieve high performance PSCs, including absorption, energy level, molecular packing, and charge transport.[17–34] As seen from the point of view of a polymer side group structure design strategy, the majority of reports on side chain engineering have focused on the different lengths, positions and types of polymer side chains, which is conducive to optimizing the

[a] College of Chemistry, Xiangtan University, Key Lab of Environment-Friendly Chemistry and Application in Ministry of Education, Xiangtan 411105, China. E-mail: liuyu03b@126.com, zhuwg18@126.com; Fax: +86-731-58292251; Tel: +86-731-58293377

[b] Qingdao Institute of Bioenergy and Bioprocess Technology, Chinese Academy of Sciences, Qingdao 266101, China. E-mail: yangrq@qibebt.ac.cn

[c] School of Materials of Science and Engineering, Changzhou University, Changzhou 213164, China

† Electronic supplementary information (ESI) available. See DOI: 10.1039/c6tc00353b

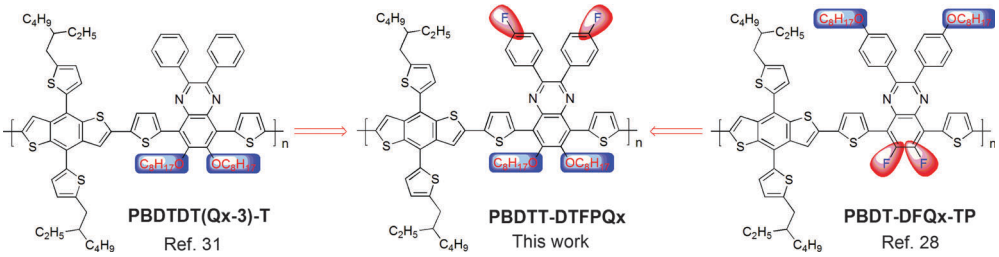

Chart 1 Chemical structures of the BDTT-*alt*-DTPQx based polymers.

molecular energy level and charge mobility, thus promoting the V_{oc} and FF of the polymer in PSCs.[15–19,22,31] For example, in polymers PBDTTPD(R_1/R_2), by adjusting the size and branching of solubilizing side chains in polymers to affect their self-assembling properties in thin film devices, and thus to promote their V_{oc} in PSCs.[15] As a result, polymer PBDTTPD(2EH/C7) has shown a maximum PCE of 8.5% with a V_{oc} of up to 0.97 V in PSCs. A polymer of PBDTT-*S*-TT with an alkylthio substitution side chains at BDTT unit has achieved a high PCE of 8.42% with a high V_{oc} of 0.84 V.[17] Our group recently also obtained a class of 5,8-alkylthienyl benzo[1,2-*b*:4,5-*b*′]dithiophene-*alt*-quinoxaline (BDTT-*alt*-Qx) polymers,[22,31] and demonstrated that two octyloxyl groups side chains instead of fluorine and hydrogen atoms at 6,7-position of quinoxaline can improve V_{oc} value in PSCs due to reducing of the HOMO levels. Moreover, in most cases, polymers introducing fluorine atoms into the acceptor units can decrease the HOMO level and further promote the charge mobility, due to the inter and intramolecular F–H hydrogen bonding effect and the induced dipole along C–F bonding to facilitate better π–π stacking and increase backbone ordering, which is conducive to promoting the FF of the polymer in PSCs.[16,25–27] Meanwhile, as a result, the FF and PCE values of the corresponding devices are promoted, while the other properties of the polymers are not significantly affected, such as optical absorption, steric hindrance, *etc.*[20,21] For example, the polymer of PPDT2FBT showed a promotion of the hole mobility with an increase of the number of fluorine atoms, and the PSCs based on PPDT2FBT/$PC_{71}BM$ demonstrated a high FF of 73%, leading to a higher PCE of 9.39%.[20] Similar phenomena have been observed in some other fluorinated D–A polymer systems.[16,25–27] Obviously, fluorination is an effective method of promoting the charge mobility of polymers, and thus improving their photovoltaic properties.

Recently, some modification of the fluorine atoms at the acceptor units in the polymer backbone has been reported.[35–38] However, fluorination at the acceptor units far away from the polymer skeleton has not been reported, although some researchers have reported that some polymers were substituted by fluorine atoms at the donor units far away from the backbone.[26,39,40] So, how to extend the application of the fluorination in D–A polymers is still of great interest and also of significant importance to the molecular design of highly efficient photovoltaic polymers.

Prompted by the abovementioned considerations, in this work, a novel D–π–A type polymer of **PBDTT-DTFPQx** based on BDTT and 2,3-bis(4-fluorophenyl)-6,7-bis(octyloxy)quinoxaline (FPQx) with thiophene as π-bridge, was synthesized and characterized. As shown in Chart 1, compared to the reported analogic polymers,[28,31] this polymer was appended with two octyloxy side chains at the 6,7-positions of quinoxaline and two fluorine atoms at the 4-position of phenyl. As reported in the literature, the presence of two 6,7-dioctyloxy groups at quinoxaline can twist the polymer backbone somehow, which can reduce the HOMO energy level and improve the V_{oc}.[22,31] The introduction of two fluorine atoms onto phenyl away from the polymer backbone not only slightly promotes the electron-withdrawing ability of quinoxaline to broaden the absorption spectrum, but also can avoid the inductive electron-withdrawing effect of the fluorine atom on the aromatic ring of the conjugated polymer backbone, leading to a widening of E_g^{opt}.[6,41] Obviously, the addition of fluorine atoms onto the phenyl can improve carrier mobility and lead to an increase in the FF value of the polymer.[6,36] Herein, we expected that the new 6,7-dioctyloxyquinoxaline derivative with 4-fluorophenyl substitution can improve photovoltaic performance along with imparting a more effective balance among the three factors of J_{sc}, V_{oc} and FF of their polymers in PSCs.

The synthetic routes of **PBDTT-DTFPQx** are shown in Scheme 1. The polymer shows a low HOMO energy level of −5.52 eV, a narrow band gap of 1.66 eV, and a hole mobility of 5.05×10^{-4} cm^2 V^{-1} s^{-1}, respectively. As expected, with an optimized blend ratio of **PBDTT-DTFPQx**:$PC_{71}BM$ (1 : 4, w/w), a high PCE of 7.2% was obtained, with a V_{oc} of 0.87 V, J_{sc} of 11.4 mA cm^{-2} and FF of 73% under AM 1.5G irradiation. The resulting copolymer reveals an outstanding FF value, and to the best of our knowledge, the maximum FF value here is one of the highest of the previous BDTT-*alt*-DTQx polymeric derivatives in BHJ-PSCs.[28,31] This work demonstrates that photovoltaic properties of the BDTT-*alt*-DTQx type polymers based PSCs can be effectively promoted by introducing 4-fluorophenyl and octyloxy substitutions at the 2,3-positions and 6,7-positions of quinoxaline.

2. Experimental section

2.1. Materials

Monomer 4,7-bis(5-bromothiophen-2-yl)-5,6-bis(octyloxy)benzo[*c*][1,2,5]thiadiazole (**1**), 1,2-bis(4-fluorophenyl)ethane-1,2-dione (**3**) and 2,5-bis(trimethyltin)-7,8-bis(5-(2-ethylhexyl)thiophen-2-yl)-benzo[1,2-*b*:4,5-*b*′]dithiophene (**BDTT-Sn_2Me_6**) were purchased directly from the Suna Tech Inc. The other reagents and

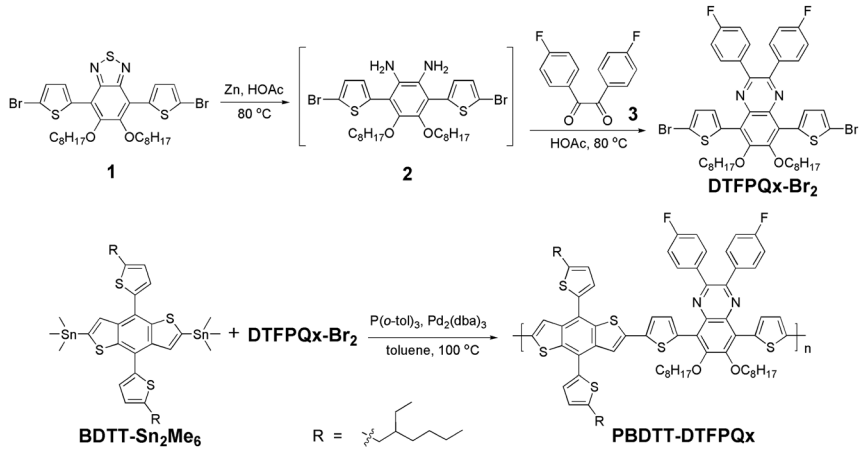

Scheme 1 Synthetic routes for the monomers and **PBDTT-DTFPQx**.

chemicals were purchased from commercial sources (Acros, TCI) and used without further purification. Compound **2** and **DTFPQx-Br$_2$** were synthesized according to the reported literature.[42] The detailed syntheses of monomers and polymer are presented following the procedures described herein.

2.2. Characterization

Nuclear magnetic resonance (NMR) spectra were recorded on a Bruker AV-400 spectrometer using tetramethylsilane (TMS) as a reference in deuterated chloroform solution at 298 K. Mass spectrometric measurements were performed on a Bruker Bifiex III MALDI-TOF. The molecular weights were determined using a Waters GPC 2410 in tetrahydrofuran (THF) *via* a calibration curve of polystyrene as standard. Thermogravimetric analyses (TGA) were conducted under a dry nitrogen gas flow at a heating rate of 20 °C min^{-1} on a Perkin-Elmer TGA 7. Differential scan calorimetry (DSC) measurements were carried out with a Netzsch DSC-204 under N_2 flow at heating and cooling rates of 10 °C min^{-1}. UV-Vis absorption spectra were recorded on a HP-8453 UV visible system. Cyclic voltammograms (CV) were carried out on a CHI660A electrochemical work station with a three electrode electrochemical cell in a 0.1 M tetrabutylammonium hexafluorophosphate ($TBAPF_6$) acetonitrile solution with a scan rate of 100 mV s^{-1} at room temperature (RT) under an argon atmosphere. In this three-electrode cell, a platinum rod, platinum wire and Ag/AgCl electrode were used as a working electrode, counter electrode and reference electrode, respectively. The surface morphology of the **PBDTT-DTFPQx**/$PC_{71}BM$ blend film was investigated by atomic force microscopy (AFM) on a Veeco, DI multimode NS-3D apparatus in tapping mode under normal air conditions at RT with a 5 μm scanner. Transmission electron microscopy (TEM) was performed using a Tecnai G2F20S-TWIN transmission electron microscope operated at an acceleration voltage of 100 kV. The HOMO and LUMO distributions of polymers were calculated by the density functional theory (DFT) (B3LYP; 6-31G*) method.

2.3. Fabrication and characterization of PSCs

The PSCs were fabricated using indium tin oxide (ITO) glass as an anode, Ca/Al as a cathode, and a blend film of the **PBDTT-DTFPQx**/$PC_{71}BM$ as a photosensitive layer. After a 30 nm buffer layer of poly(3,4-ethylenedioxy-thiophene) and polystyrene sulfonic acid (PEDOT:PSS) was spin-coated onto the precleaned ITO substrate, the photosensitive layer was subsequently prepared by spin-coating a solution of the **PBDTT-DTFPQx**/$PC_{71}BM$ (1 : 4, w/w) in 1,2-dichlorobenzene (ODCB) with 1% DIO (DIO/ODCB, v/v) on the PEDOT:PSS layer with a typical concentration of 35 mg mL^{-1}, followed by annealing at 80 °C for 10 minutes. Ca (10 nm) and Al (100 nm) were successively deposited on the photosensitive layer in vacuum and used as top electrodes. The current–voltage (*I–V*) characterization of the devices was carried out on a computer-controlled Keithley source measurement system. A solar simulator was used as the light source and the light intensity was monitored by a standard Si solar cell. The active area was 4×10^{-2} cm^2 for each cell. The thicknesses of the spun-cast films were recorded by a profilometer (Alpha-Step 200, Tencor Instruments). The external quantum efficiency (EQE) was measured with a Stanford Research Systems model SR830 DSP lock-in amplifier coupled with WDG3 monochromator and a 150 W xenon lamp.

2.4. Synthesis of the monomer and polymer

2.4.1. 5,8-Bis(5-bromothiophen-2-yl)-2,3-bis(4-fluorophenyl)-6,7-bis(octyloxy)quinoxaline (DTFPQx-Br$_2$). Compound **1** (0.71 g, 1.00 mmol) and zinc powder (0.78 g, 12.00 mmol) were mixed with acetic acid (HOAc, 100 mL), and stirred for 2 h at 80 °C under nitrogen atmosphere. After being cooled to RT, the mixture is filtered and washed with HOAc. The organic phase containing compound **2** of 3,6-bis(5-bromothiophen-2-yl)-4,5-bis(octyloxy)benzene-1,2-diamine was obtained and directly used in the next step. The organic phase was added HOAc (100 mL) and compound **3** (0.25 g, 1.00 mmol). The mixture was refluxed under stirring for 12 h under a nitrogen atmosphere. After being cooled to RT and quenched with water, the mixture was then extracted with dichloromethane (DCM, 30 mL × 3). The combined organic layer was dried over anhydrous $MgSO_4$ and distilled to remove solvent. The residue was purified by silica gel column chromatography using a mixed solvent of petroleum ether (PE)–DCM (v/v, 3/1) as eluent to obtain

compound **DTFPQx-Br$_2$** as a yellow solid (0.67 g, 75%). ^{1}H NMR (400 MHz, $CDCl_3$, TMS), δ (ppm): 7.92 (d, J = 2.5 Hz, 2H), 7.61 (dd, J = 4.0, 8.0 Hz, 4H), 7.14 (d, J = 2.4 Hz, 2H), 7.08 (dd, J = 8.0, 8.0 Hz, 4H), 4.06 (t, J = 6.3 Hz, 4H), 1.83–1.80 (m, 4H), 1.42–1.30 (m, 20H), 0.89 (t, J = 6.3 Hz, 6H). ^{13}C NMR (100 MHz, $CDCl_3$, TMS), (ppm): 152.88, 149.25, 135.85, 134.97, 134.34, 132.18, 131.20, 128.97, 123.31, 116.13, 115.63, 115.40, 74.23, 31.82, 30.39, 29.44, 29.28, 26.03, 22.67, 14.11. MALDI-TOF MS (m/z) for $C_{44}H_{46}Br_2F_2N_2O_2S_2$, calcd: 898.13, found: 898.41.

2.4.2. Synthesis of PBDTT-DTFPQx. In a dry 25 mL flask, tris(dibenzylideneacetone)dipalladium ($Pd_2(dba)_3$, 5.0 mg) and tri(*o*-tolyl)phosphine (P(*o*-Tol)$_3$, 10.0 mg) were added to a solution of **DTFPQx-Br$_2$** (116 mg, 0.13 mmol) and **BDTT-Sn$_2$Me$_6$** (118 mg, 0.13 mmol) in 6 mL degassed toluene under nitrogen protect and stirred vigorously at 100 °C for 15 h until the reaction system became viscous. After cooling to RT, the mixture was poured into acetone (100 mL) to precipite the crude product. It was collected by filtration and successively extracted in a Soxhlet apparatus with diethyl ether, DCM and chloroform ($CHCl_3$) each for 12 h, respectively. The collected $CHCl_3$ solution was concentrated and precipitated with acetone to obtain a dark solid (141 mg, 83%). ^{1}H NMR (400 MHz, $CDCl_3$, TMS), δ (ppm): 8.18–8.16 (br, 2H), 7.80–7.77 (br, 6H), 7.43–7.37 (br, 4H), 7.06–7.00 (br, 6H), 4.14–4.13 (br, 4H), 2.96–2.94 (br, 4H), 2.02–2.01 (br, 2H), 1.87–1.86 (br, 4H), 1.75–1.74 (br, 2H), 1.46–1.26 (br, 34H), 0.99–0.87 (br, 18H). Anal. calcd for $C_{78}H_{88}F_2N_2O_2S_6$: C, 71.19; H, 6.74; N, 2.13; S, 14.62. Found: C, 70.05; H, 7.12; N, 2.18; S, 14.33.

3. Results and discussion

3.1. Synthesis and thermal properties

As shown in Scheme 1, compound **2** was obtained by a ring-opening reaction and used immediately to get monomer **DTFPQx-Br$_2$** *via* the condensation reaction with a yield of 75%. The polymer of **PBDTT-DTFPQx** was synthesized by palladium catalyzed Stille polymerization between **DTFPQx-Br$_2$** and **BDTT-Sn$_2$Me$_6$** with a yield of 83%. The chemical structure of monomer **DTFPQx-Br$_2$** was confirmed by ^{1}H NMR, ^{13}C NMR and MALDI-TOF mass spectroscopy. Furthermore, polymer **PBDTT-DTFPQx** was characterized by ^{1}H NMR and elemental analysis. The number-average molecular weight (M_n), weight-average molecular weight (M_w) and the polydispersity index (PDI) of the polymer were observed by GPC measurement, showing that the M_n value is 43.1 kDa with a PDI of 1.88 (Table 1). **PBDTT-DTFPQx** exhibits excellent solubility in common organic solvents, such as THF, $CHCl_3$, chlorobenzene (CB) and ODCB, due to the influence of the appended two octyloxy side chains at quinoxaline. The thermal properties of **PBDTT-DTFPQx** were investigated by TGA and DSC. As shown in Fig. S1 (ESI†), **PBDTT-DTFPQx** presents good thermal stability, with 5% weight-loss temperatures (T_d) at 332 °C under an inert atmosphere (Table 1). Fig. S2 (ESI†) depicts the curve from DSC. There was no obvious thermal transition temperature (T_g) and crystallization temperature (T_c) for **PBDTT-DTFPQx**.

Table 1 Molecular weight and thermal properties of **PBDTT-DTFPQx**

Polymers	M_n (kDa)	M_w (kDa)	PDI	Yield (%)	T_d (°C)
PBDTT-DTFPQx	43.1	81.0	1.88	83	332

3.2. Optical properties

The absorption spectra of the polymer, both in $CHCl_3$ solution (1×10^{-5} M) and in the solid state, are shown in Fig. 1, and their detailed absorption data are summarized in Table 2. Two typical and obvious absorption bands are observed in the range of 300–750 nm for the polymer. The high-lying absorption band from 300 to 450 nm is attributed to the π–π* transition, and another low-lying absorption band from 500 to 750 nm should assigned be to the strong intramolecular charge transfer (ICT) interaction between electron-rich moiety (BDTT) and the electron-deficient moiety (FPQx).[31,43] Compared to the absorption profiles in solution, those in thin films exhibited a significant red-shift up to 83 nm, which is probably caused by the strong intermolecular π–π stacking interaction. The absorption edge (λ_{onset}) of **PBDTT-DTFPQx** is located at 745 nm in its thin film, corresponding to the optical band gap (E_g^{opt}) of 1.66 eV. Obviously, compared to the previous analogues of **PBDT-DFQX-TP** and **PBDTDT(Qx-3)-T** (both E_g^{opt} of 1.78 eV),[28,31] **PBDTT-DTFPQx** can well enhance the ICT effect and broaden the absorption spectrum, which can result in a lower E_g^{opt} and higher J_{sc} value.[6,31]

3.3. Electrochemical properties

The electrochemical properties of **PBDTT-DTFPQx** were investigated by cyclic voltammetry (CV) using an Ag/AgCl electrode as a reference and the redox potential of ferrocene/ferrocenium (Fc/Fc^+) as a calibrated standard. Fig. 2 shows the recorded CV curve of **PBDTT-DTFPQx**, and the corresponding CV data are summarized in Table 2. The observed onset oxidation potential (E_{ox}) for **PBDTT-DTFPQx** is 1.17 V, and the corresponding HOMO energy level (E_{HOMO}) is estimated to be −5.52 eV according to the empirical equations:[31] $E_{HOMO} = -(E_{ox} - 0.45) - 4.8$ eV. Obviously, **PBDTT-DTFPQx** presents a lower E_{HOMO} value than those of the

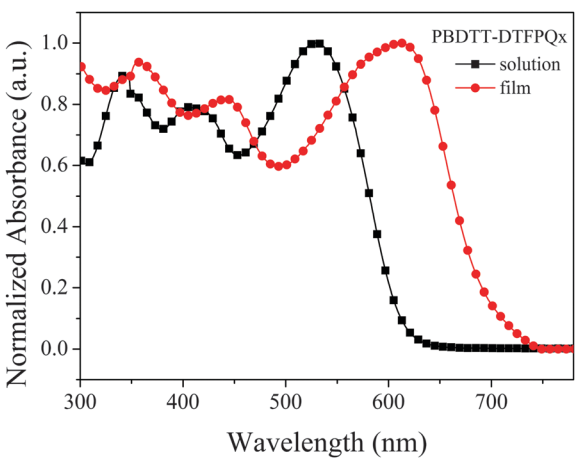

Fig. 1 Normalized UV-Vis absorption spectra of **PBDTT-DTFPQx** in dilute $CHCl_3$ and its neat film at RT.

Table 2 Optical and electrochemical properties of **PBDTT-DTFPQx**

Polymers	$\lambda_{abs}{}^{a}$/nm	$\lambda_{abs}{}^{b}$/nm	$\lambda_{onset}{}^{b}$/nm	E_g^{opt}/eV	E_{HOMO}/eV	Ref.
PBDTT-DTFPQx	342, 413, 531	359, 443, 614	745	1.66	−5.52	This work
PBDT-DFQX-TP	347, 418, 559	359, 431, 583	695	1.78	−5.25	28
PBDTDT(Qx-3)-T	408, 526	438, 577	696	1.78	−5.51	31

[a] Measured in $CHCl_3$ solution. [b] Measured in the neat film.

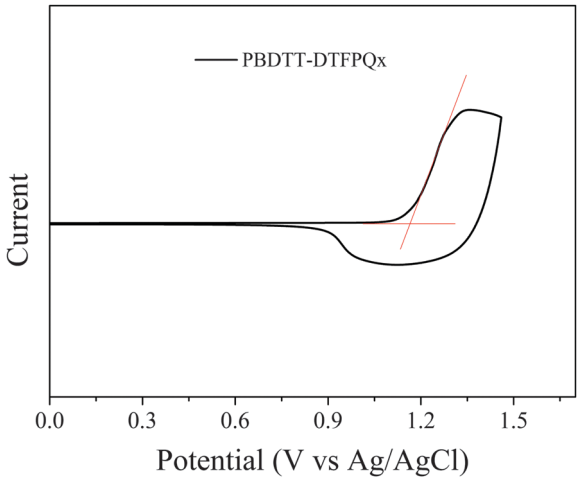

Fig. 2 Cyclic voltammetry curve of **PBDTT-DTFPQx**.

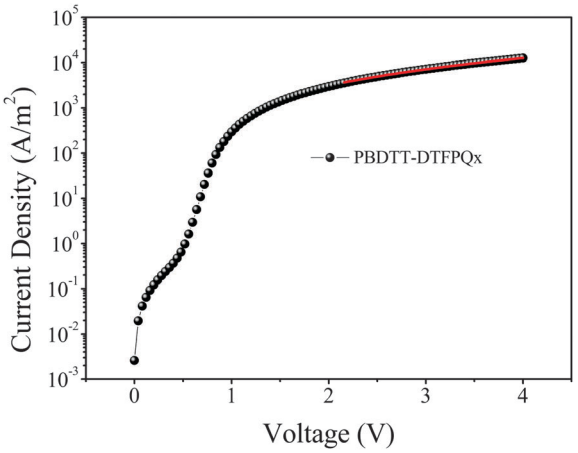

Fig. 3 *J–V* curve of the hole **PBDTT-DTFPQx**/$PC_{71}BM$ device at optimized conditions.

previous analogues,[22,28,31] that is to say, grafting two fluorine atoms at the phenyl can slightly increase the electron withdrawing ability of quinoxaline, and cause a lower HOMO level for **PBDTT-DTFPQx**. On the other hand, a similar HOMO energy level for **PBDTT-DTFPQx** and **PBDTDT(Qx-3)-T** (−5.51 eV) was observed, implying that the introduction of two fluorine atoms at the phenyl away from the conjugated backbone has little influence on the HOMO energy level of the polymer.[31] The results are consistent with the DFT calculation of polymers (Fig. S3, see ESI†).

3.4. Hole mobility

The charge transport properties of polymers have an important effect on the resulting photovoltaic performance of PSCs, especially on FF.[16,27] We measured the hole-only mobilities (μ_h) of **PBDTT-DTFPQx** blended with $PC_{71}BM$ at optimized conditions by the space charge limited current (SCLC) method with a typical device structure of ITO/PEDOT:PSS/polymer:$PC_{71}BM$/Au. The SCLC could be estimated using the Mott–Gurney equation: $J = (9/8)\varepsilon_0\varepsilon_r\mu_h(V^2/L^3)$,[43,44] where, J is current density, ε_r is dielectric constant of polymer (3.0), ε_0 is free-space permittivity (8.85×10^{-12} F m^{-1}), L is thickness of the blended film layer (124 nm), $V = V_{appl} - V_{bi}$, V is the effective voltage, V_{appl} is applied voltage, and V_{bi} is built-in voltage that results from the work function difference between the anode and cathode. As shown in Fig. 3, the μ_h of **PBDTT-DTFPQx** was calculated to be 5.05×10^{-4} cm^2 V^{-1} s^{-1} in the hole-only device, which is 2.3 times higher than that of the analogue **PBDTDT(Qx-3)-T**.[31] Obviously, the μ_h of **PBDTT-DTFPQx** shows a certain increase, which implies that a relatively higher FF could be obtained in the PSCs.[16,40]

3.5. Photovoltaic properties

To investigate the photovoltaic properties of **PBDTT-DTFPQx**, the BHJ PSCs were also fabricated with a typical device structure of ITO/PEDOT:PSS/active layer/Ca/Al. The active layer of **PBDTT-DTFPQx**/$PC_{71}BM$ was obtained from an ODCB solution at a concentration of 35 mg mL^{-1}. As demonstrated, the photovoltaic performances of PSCs are strongly affected by the processing parameters,[45] including the D/A ratio (w/w), annealing temperature, DIO additive concentration and spin-coating rate, and these optimized parameters were obtained and are shown in Fig. S4, S5, S6 and S7 (see ESI†), respectively. The corresponding photovoltaic data are summarized in Tables S1, S2, S3 and S4 (see ESI†), respectively. As a result, the **PBDTT-DTFPQx**/$PC_{71}BM$ based PSCs have an optimized D/A ratio of 1 : 4, annealing temperature of 80 °C, DIO additive concentration of 1% and spin-coating rate of 2250 rpm, respectively. As shown in Fig. 4, the PSCs exhibited the typical *J–V* characteristics under optimized conditions, and the device parameters, such as J_{sc}, V_{oc}, FF and PCE were summarized in Table 3. Encouragingly, the **PBDTT-DTFPQx**/$PC_{71}BM$-based PSCs showed outstanding photovoltaic performance, in which the maximum PCE of 7.2% with a V_{oc} of 0.87 V, a J_{sc} of 11.4 mA cm^{-2}, and a FF of up to 73% was achieved. To our knowledge, the recorded maximum FF value here is one of the highest of the previous quinoxaline based on copolymeric derivatives in BHJ PSCs.[28,40,46] The results indicate that molecular modification by introducing two octyloxy side chains at the 6,7-positions of quinoxaline and two fluorine atoms at the 4-position of phenyl onto quinoxaline will be a promising strategy to decrease the HOMO level and increase the μ_h of the low bandgap conjugated polymers, and for further enhancing

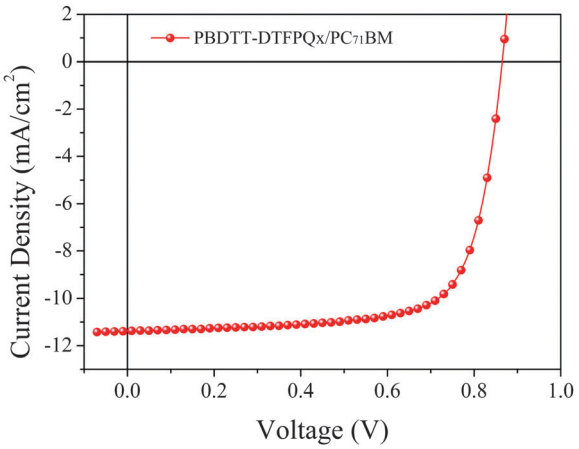

Fig. 4 *J*–*V* curves of the **PBDTT-DTFPQx**/$PC_{71}BM$-based PSCs at optimized conditions under illumination of AM 1.5G, 100 mW cm^{-2}.

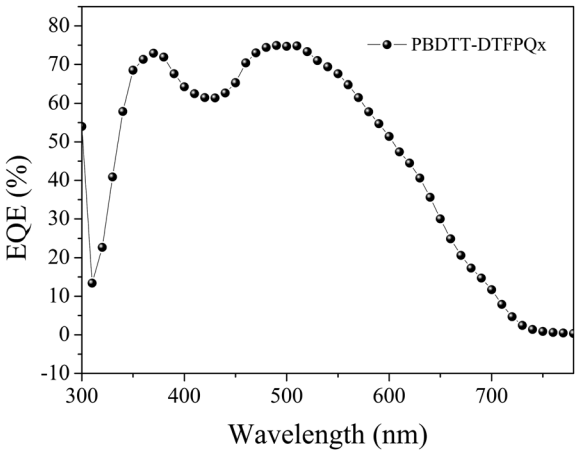

Fig. 5 EQE curves of the **PBDTT-DTFPQx**/$PC_{71}BM$-based devices under the optimized conditions.

Table 3 Photovoltaic properties of the BDTT-*alt*-DTPQx polymers based PSCs under illumination of AM 1.5G, 100 mW cm^{-2}

Polymers	J_{sc}/ mA cm^{-2}	V_{oc}/V	FF/%	PCE_{max} (PCE_{ave}[b])/%	μ_h/ cm^2 V^{-1} s^{-1}	Ref.
PBDTT-DTFPQx[a]	11.4	0.87	73	7.2 (7.0)	5.05×10^{-4}	This work
PBDT-DFQX-TP	12.34	0.82	60.12	6.08	1.33×10^{-3}	28
PBDTDT(Qx-3)-T[a]	11.28	0.94	64.7	6.9	2.19×10^{-4}	31

[a] With thermal annealing at 80 °C for 10 min and 1% DIO. [b] The average PCE was obtained from over 10 devices.

the photovoltaic performance of PSCs. Notably, compared to the non-fluorine substituted analogue **PBDTDT(Qx-3)-T**,[31] **PBDTT-DTFPQx** shows a reduced V_{oc}, although both have similar HOMO levels. This apparent anomaly may be attributable to the relatively poor solubility of **PBDTT-DTFPQx**,[47] and due to the V_{oc} being determined by the charge transfer complex formation between polymer and the fullerene. However, the relatively poor solubility of **PBDTT-DTFPQx** hampered the charge recombination at the D/A interface, leading to a low V_{oc}.[48]

To understand why the **PBDTT-DTFPQx**/$PC_{71}BM$ based devices displayed high PCE values, the external quantum efficiency (EQE) curves of devices under the optimized conditions were also measured. As depicted in Fig. 5, the **PBDTT-DTFPQx**/$PC_{71}BM$ based device show very efficient photo-response in a broad range from 300 to 740 nm, corresponding to high EQE over 40% in a broad range from 328 to 632 nm, with the maximum EQE of 75% being observed at 510 nm. Obviously, the high EQE value is responsible for the high J_{sc} of **PBDTT-DTFPQx** based PSCs. According to the EQE curve and the solar irradiation spectrum, the integral J_{sc} value of the **PBDTT-DTFPQx** based PSC is 11.1 mA cm^{-2}, which is coincident with the measured J_{sc} value within a 3% error. This indicates that our photovoltaic measurement is accurate and reliable.

3.6. Morphology

The AFM and the TEM measurements were carried out to demonstrate the surface and internal morphologies of the **PBDTT-DTFPQx**/$PC_{71}BM$ (1 : 4, w/w) blend films processed without post processing, or by annealing or annealing with 1% DIO additive. The height images (5 × 5 μm^2) are shown in Fig. 6, and the corresponding the root mean square (RMS) roughnesses are observed to be 1.59, 0.97, 0.68 nm in the films without post processing, annealing and annealing with 1% DIO additive, respectively. A good surface morphology is available to enhance the photovoltaic performance of the corresponding device due to the promotion of the exciton dissociation and charge transportation. Fig. 6 also shows TEM images of the blended films. The dark areas in the TEM images are attributed to $PC_{71}BM$-rich domains, and the bright regions to the polymer-rich domains. It is obvious that the film without any extra processing showed a poor phase separation. After annealing or DIO treatment, the blend films showed the bicontinuous D/A interpenetrating network. The well-developed fibrillar structure and suitable fiber size, which would be beneficial to efficient exciton dissociation and charge transportation, and thus higher PCE value can be harvested. The results agreed well with an improvement of FF from 51% to 73% for the **PBDTT-DTFPQx** based PSCs, and the best device had a high PCE of up to 7.2%. Therefore, the relatively excellent morphology together with good hole mobility mentioned above, results in an outstanding FF and a higher PCE values.

3.7. XRD analysis

The XRD patterns of polymers were recorded to investigate the molecular interactions in detail and they are shown in Fig. 7. It is observed that fluorinated **PBDTT-DTFPQx** and its non-fluorinated analogue **PBDTDT(Qx-3)-T** show a strong peak at 2θ = 22.6° and 2θ = 22.1°, respectively, indicating that the two polymers have effective π–π stacking. Compared with **PBDTDT(Qx-3)-T**,[31] **PBDTT-DTFPQx** exhibited an increased 2θ peak. This implies that incorporating the fluorine atom at the 4-phenyl of quinoxaline would enhance intermolecular π–π stacking, which is in favor of exciton dissociation and charge transportation, offering a largely higher J_{sc} and FF in the

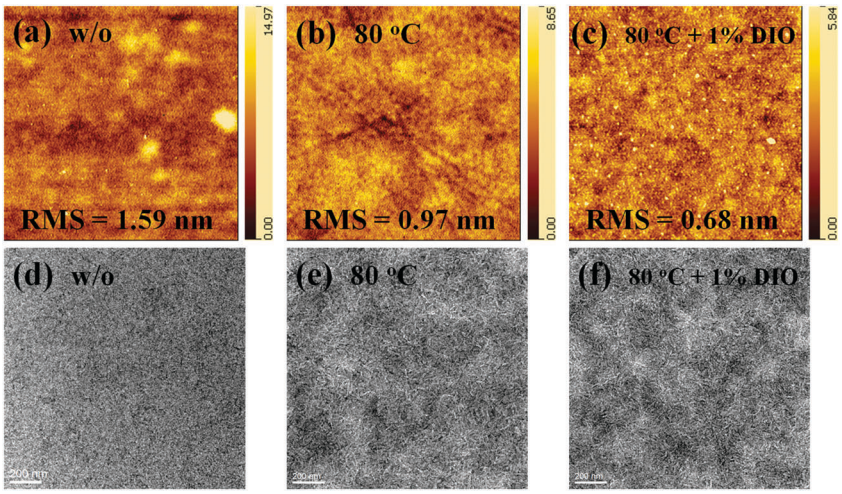

Fig. 6 AFM height images, TEM images of the **PBDTT-DTFPQx**/$PC_{71}BM$ blend films without post processing (a and d), with annealing at 80 °C (b and e), and with annealing at 80 °C with 1% DIO additive (c and f), respectively.

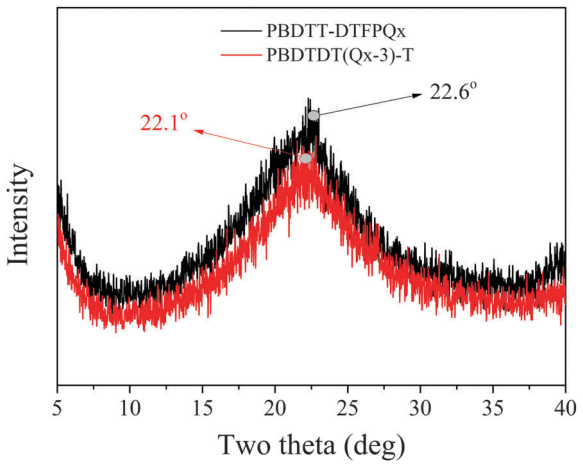

Fig. 7 XRD spectra of the polymers thin films.

resulting devices.[49] Obviously, this is consistent with the results of UV-vis absorption and charge carrier mobility measurements of polymers.

4. Conclusions

In conclusion, a novel D–π–A type polymer of **PBDTT-DTFPQx** was synthesized. **PBDTT-DTFPQx** exhibited a broad absorption in the range of 300–745 nm, a low-lying HOMO energy level of −5.52 eV, and a good carrier mobility of 5.05×10^{-4} cm^2 V^{-1} s^{-1}. The PSCs based on **PBDTT-DTFPQx** exhibited an outstanding FF of 73%, which is among one of the highest of the reported polymers based quinoxaline. As a result, a high PCE of 7.2% was obtained, with a V_{oc} of 0.87 V and a J_{sc} of 11.4 mA cm^{-2}. The results indicate that incorporation of two electron-withdrawing fluoride atoms onto the 4-positions of the phenyl at the quinoxaline unit by side-chain engineering would be a feasible approach to improve photovoltaic properties for the BDTT-*alt*-DTQx type polymer based PSCs.

Acknowledgements

Thanks to the financial supports from the Major Cultivation and General Programs of the National Natural Science Foundation of China (51573154, 91233112, 51273168, 51403178), the Program for Innovative Research Cultivation Team in University of Ministry of Education of China (1337304), the Innovation Group in Hunan Natural Science Foundation (12JJ7002), the Natural Science Foundation of Hunan (14JJ4019, 2015JJ3113), Research Foundation of Hunan Education Bureau (13A102, 14C1099), Open Project for the National Key Laboratory of Luminescent Materials and Devices (2014-skllmd-10).

Notes and references

1 Y. Li, *Acc. Chem. Res.*, 2012, **45**, 723.
2 J. S. Wu, S. W. Cheng, Y. J. Cheng and C. S. Hsu, *Chem. Soc. Rev.*, 2015, **44**, 1113.
3 Z. G. Zhang and Y. F. Li, *Sci. China: Chem.*, 2015, **58**, 192.
4 E. G. Wang, W. Mammo and M. R. Andersson, *Adv. Mater.*, 2014, **26**, 1801.
5 C. Lu, H. Chen, W. Chuang, Y. Hsu, W. Chen and P. Chou, *Chem. Mater.*, 2015, **27**, 6837.
6 Y. Li, B. Meng, H. Tong, Z. Y. Xie and L. X. Wang, *Polym. Chem.*, 2014, **5**, 1848.
7 X. Guo, M. J. Zhang, J. H. Tan, S. Q. Zhang, L. J. Huo, W. P. Hu, Y. F. Li and J. H. Hou, *Adv. Mater.*, 2012, **24**, 6536.
8 Z. Zhang, F. Lin, H. Chen, H. Wu, C. Chung, C. Lu, S. Liu, S. Tung, W. Chen, K. Wong and P. Chou, *Energy Environ. Sci.*, 2015, **8**, 552.
9 Q. Fan, Y. Liu, P. Yang, W. Su, M. Xiao, J. Chen, M. Li, X. Wang, Y. Wang, H. Tan, R. Yang and W. Zhu, *Org. Electron.*, 2015, **23**, 124.
10 Y. Liu, J. Zhao, Z. Li, C. Mu, W. Ma, H. Hu, K. Jiang, H. Lin, H. Ade and H. Yan, *Nat. Commun.*, 2014, **5**, 6293.

11 J. Warnan, A. E. Labban, C. Cabanetos, E. T. Hoke, P. K. Shukla, C. Risko, J. L. Brédas, M. D. McGehee and P. M. Beaujuge, *Chem. Mater.*, 2014, **26**, 2299.
12 W. Y. Su, Q. P. Fan, M. J. Xiao, J. H. Chen, P. Zhou, B. Liu, H. Tan, Y. Liu, R. Q. Yang and W. G. Zhu, *Macromol. Chem. Phys.*, 2014, **215**, 2075.
13 A. Casey, R. S. Ashraf, Z. P. Fei and M. Heeney, *Macromolecules*, 2014, **47**, 2279.
14 H. Li, S. Sun, S. Mhaisalkar, M. T. Zin, Y. M. Lam and A. C. Grimsdale, *J. Mater. Chem. A*, 2014, **2**, 17925.
15 C. Cabanetos, A. E. Labban, J. A. Bartelt, W. R. Mateker, J. M. J. Fréchet, M. D. McGehee and P. M. Beaujuge, *J. Am. Chem. Soc.*, 2013, **135**, 4656.
16 W. Li, S. Albrecht, L. Yang, S. Roland, J. R. Tumbleston, T. McAfee, L. Yan, M. A. Kelly, H. Ade, D. Neher and W. You, *J. Am. Chem. Soc.*, 2014, **136**, 15566.
17 C. H. Cui, W. Y. Wong and Y. F. Li, *Energy Environ. Sci.*, 2014, **7**, 2276.
18 X. C. Wang, Z. G. Zhang, H. Luo, S. Chen, S. Q. Yu, H. Q. Wang, X. Y. Li, G. Yu and Y. F. Li, *Polym. Chem.*, 2014, **5**, 502.
19 P. Yang, M. Yuan, D. F. Zeigler, S. E. Watkins, J. A. Lee and C. K. Luscombe, *J. Mater. Chem. C*, 2014, **2**, 3278.
20 T. L. Nguyen, H. Choi, S. J. Ko, B. Walker, S. Yum, M. H. Yun, T. J. Shin, S. Hwang, J. Y. Kim and H. Y. Woo, *Energy Environ. Sci.*, 2014, **7**, 3040.
21 T. Qin, W. Zajaczkowski, W. Pisula, M. Baumgarten, M. Chen, M. Gao, G. Wilson, C. D. Easton, K. Müllen and S. E. Watkins, *J. Am. Chem. Soc.*, 2014, **136**, 6049.
22 W. Su, M. Xiao, Q. Fan, J. Zhong, J. Chen, D. Dang, J. Shi, W. Xiong, X. Duan, H. Tan, Y. Liu and W. Zhu, *Org. Electron.*, 2015, **17**, 129.
23 Y. Deng, J. Liu, J. Wang, L. Liu, W. Li, H. Tian, X. Zhang, Z. Xie, Y. Geng and F. Wang, *Adv. Mater.*, 2014, **26**, 471.
24 J. Wang, M. Xiao, W. Chen, M. Qiu, Z. Du, W. Zhu, S. Wen, N. Wang and R. Yang, *Macromolecules*, 2014, **47**, 7823.
25 J. Jheng, Y. Lai, J. Wu, Y. Chao, C. Wang and C. Hsu, *Adv. Mater.*, 2013, **25**, 2445.
26 M. Zhang, X. Guo, S. Zhang and J. Hou, *Adv. Mater.*, 2014, **26**, 1118.
27 J. W. Jo, J. W. Jung, E. H. Jung, H. Ahn, T. J. Shin and W. H. Jo, *Energy Environ. Sci.*, 2015, **8**, 2427.
28 M. Wang, D. Ma, K. Shi, S. Shi, S. Chen, C. Huang, Z. Qiao, Z. G. Zhang, Y. Li, X. Li and H. Wang, *J. Mater. Chem. A*, 2015, **3**, 2802.
29 L. Ye, S. Zhang, W. Zhao, H. Yao and J. Hou, *Chem. Mater.*, 2014, **26**, 3603.
30 M. Zhang, Y. Gu, X. Guo, F. Liu, S. Zhang, L. Huo, T. P. Russell and J. Hou, *Adv. Mater.*, 2013, **25**, 4944.
31 Q. P. Fan, M. Xiao, Y. Liu, W. Su, H. Gao, H. Tan, Y. Wang, G. Lei, R. Yang and W. Zhu, *Polym. Chem.*, 2015, **6**, 4290.
32 L. Ye, S. Zhang, L. Huo, M. Zhang and J. Hou, *Acc. Chem. Res.*, 2014, **47**, 1595.
33 K. Mahmood, H. Lu, Z. P. Liu, C. Li, Z. Lu, X. Liu, T. Fang, Q. Peng, G. Li, L. Li and Z. Bo, *Polym. Chem.*, 2014, **5**, 5037.
34 K. R. Graham, C. Cabanetos, J. P. Jahnke, M. N. Idso, A. E. Labban, G. O. N. Ndjawa, T. Heumueller, K. Vandewal, A. Salleo, B. F. Chmelka, A. Amassian, P. M. Beaujuge and M. D. McGehee, *J. Am. Chem. Soc.*, 2014, **136**, 9608.
35 H. Chen, Y. Chen, C. Liu, Y. Hsu, Y. Chien, W. Chuang, C. Cheng, C. Liu, S. Chou, S. Tung and P. Chou, *Polym. Chem.*, 2013, **4**, 3411.
36 A. C. Stuart, J. R. Tumbleston, H. Zhou, W. Li, S. Liu, H. Ade and W. You, *J. Am. Chem. Soc.*, 2013, **135**, 1806.
37 F. Meyer, *Prog. Polym. Sci.*, 2015, **47**, 70.
38 H. C. Chen, Y. H. Chen, C. C. Liu, Y. C. Chien, S. W. Chou and P. T. Chou, *Chem. Mater.*, 2012, **24**, 4766.
39 W. Chen, Z. Du, L. Han, M. Xiao, W. Shen, T. Wang, Y. Zhou and R. Yang, *J. Mater. Chem. A*, 2015, **3**, 3130.
40 D. Liu, W. Zhao, S. Zhang, L. Ye, Z. Zheng, Y. Cui, Y. Chen and J. Hou, *Macromolecules*, 2015, **48**, 5172.
41 J. W. Jung, F. Liu, T. P. Russell and W. H. Jo, *Adv. Energy Mater.*, 2015, **5**, 1500065.
42 Q. Fan, Y. Liu, M. Xiao, H. Tan, Y. Wang, W. Su, D. Yu, R. Yang and W. Zhu, *Org. Electron.*, 2014, **15**, 3375.
43 P. W. M. Blom, V. D. Mihailetchi, L. J. A. Koster and D. E. Markov, *Adv. Mater.*, 2007, **19**, 1551.
44 A. M. Goodman and A. Rose, *J. Appl. Phys.*, 1971, **42**, 2823.
45 Q. P. Fan, X. Xu, Y. Liu, W. Su, X. He, Y. Zhang, H. Tan, Y. Wang, Q. Peng and W. G. Zhu, *Polym. Chem.*, 2016, **7**, 1747.
46 H. Wu, B. Zhao, W. Wang, Z. Guo, W. Wei, Z. An, C. Gao, H. Chen, B. Xiao, Y. Xie, H. Wu and Y. Cao, *J. Mater. Chem. A*, 2015, **3**, 18115.
47 Y. Wang, X. Xin, Y. Lu, T. Xiao, X. Xu, N. Zhao, X. Hu, B. S. Ong and S. C. Ng, *Macromolecules*, 2013, **46**, 9587.
48 J. J. B. Smith, L. Goris, K. Vandewal, K. Haenen, J. V. Manca, D. Vanderzande, D. D. C. Bradley and J. Nelson, *Adv. Funct. Mater.*, 2007, **17**, 451.
49 Q. P. Fan, Y. Liu, M. Xiao, W. Y. Su, H. Gao, J. Chen, H. Tan, Y. Wang, R. Q. Yang and W. G. Zhu, *J. Mater. Chem. C*, 2015, **3**, 6240.